

VĚDECKÉ SPISY VYSOKÉHO UČENÍ TECHNICKÉHO V BRNĚ

Edice PhD Thesis, sv. 863

ISSN 1213-4198

thesis
IS

Ing. Stanislav Žák

**Deformation and Stress Fields
at the Front of Shear Cracks
with Complicated Geometry**



CENTRAL EUROPEAN INSTITUTE OF TECHNOLOGY

STŘEDOEVROPSKÝ TECHNOLOGICKÝ INSTITUT

**DEFORMATION AND STRESS FIELDS AT THE FRONT
OF SHEAR CRACKS WITH COMPLICATED GEOMETRY**

POLE NAPĚTÍ A DEFORMACE V OKOLÍ TRHLIN S KOMPLIKOVANOU
GEOMETRIÍ ČELA ZATÍŽENÝCH VE SMYKOVÝCH ZÁTĚŽNÝCH MÓDECH

ZKRÁCENÁ VERZE PH.D. THESIS

OBOR	Pokročilé materiály
AUTOR PRÁCE	Ing. Stanislav Žák
ŠKOLITEL	doc. Ing. Jana Horníková, Ph.D.
OPONENTI	prof. Ing. Jiří Kunz, CSc. doc. Ing. Pavel Hutař, Ph.D.
DATUM OBHAJOBY	15. října 2018

Brno 2018

Keywords:

Compact-tension-shear specimen, crack tortuosity, cylindrical specimen, finite element modeling, linear-elastic fracture mechanics, shear mode loading, stress intensity factors

Klíčová slova:

CTS vzorek, křivolakost trhliny, lineárně-elastická lomová mechanika, MKP modelování, smykové zátěžné módy, součinitele intenzity napětí, válcový vzorek

MÍSTO ULOŽENÍ PRÁCE

CEITEC, Vysoké učení technické v Brně
Purkyňova 123
612 00 Brno

© Stanislav Žák, 2018

ISBN 978-80-214-5688-4

ISSN 1213-4198

TABLE OF CONTENTS

1 INTRODUCTION	5
2 THEORY	6
2.1 Influence of the crack microstructure on the fracture parameters.....	8
3 AIMS OF THE THESIS.....	9
4 USED METHODS AND MODELS	11
4.1 Cylindrical specimen.....	11
4.2 CTS specimen	12
4.3 FE modelling.....	13
5 RESULTS	15
5.1 Model simplifications (cylindrical specimen).....	15
5.2 Mode III crack propagation (cylindrical specimen).....	17
5.3 Uniform crack roughness (CTS specimen)	18
5.4 Tilt and twist of the crack front (CTS specimen).....	22
5.5 Fully random crack front and flanks geometry (CTS specimen).....	23
6 CONCLUSIONS	24
REFERENCES	26
CURRICULUM VITAE.....	29
ABSTRACT	30

1 INTRODUCTION

In recent time mankind is using more modern and advanced mechanical instruments and gadgets each day in all kinds of industrial branches. Even the smallest devices used in day-to-day applications by ordinary people are becoming very complex and complicated. This leads (almost) to addiction on the modern technologies because no-one can imagine a day, even an hour without his mobile phone, computer, car, always accessible source of electrical energy, etc. But accidents happen and none of these devices are indestructible which means that time-to-time something disturb the luxury of human life...

To improve the situation two things can be done – either to simplify everything and go “back to roots” without use of any complicated technology or to work on refining the devices to increase their durability and prolong their operating life. The second resort seems to be more useful in our modern society and mankind is working on this approach for decades.

Numerous theoretical approaches to describe fracture behavior, fatigue of materials and related material properties were developed [1] starting with the work of Inglis and Griffith in early 20th century. Their work was broadened by other different approaches [2–4] (e.g. J -integral, stress intensity factors (SIFs), crack tip opening displacement (CTOD), etc.) to evaluate the fracture parameters. These approaches were used to create models representing at first some abstract bodies with cracks (2D infinite or semi-infinite planes with central crack) but they were adapted to more real-like specimens and geometries at a very fast pace. These models are now used as a tool to obtain some description of the fracture by means of quantitative results for normalized experiments [5].

Produced models proved to be very useful when behavior of bulk materials under normalized conditions is investigated. For experimental testing of materials in terms of fracture and fatigue behavior, several simplifications can be used with very small, almost insignificant impact on investigated results. However, in cases where the influence of microstructure of material has to be accounted for, the basic fracture mechanics models fail to produce satisfactory results or to describe experimentally observed phenomena.

In more in-depth research the crack front and faces geometry cannot be assumed with simple, planar geometry. It has been shown [6–8] that fractures (particularly under the remote shear loading) exhibit geometrical changes on the microstructure level of the crack front and flanks which leads to crack front and flanks roughness.

This work aims to investigate those cases of cracked specimens where planar simplifications of the crack shape are not usable and where it would lead to some discrepancies in results. Moreover, it is aimed at those cases where the planar model cannot sufficiently describe observed phenomena. Especially the shear mode loaded cracks (when there is no mode I crack opening), which can be affected by real-like geometry of the crack.

2 THEORY

Standard approach to obtain stress and strain fields around the crack front divides loading according to deformation of the crack into three basic types – mode I (normal mode), mode II (in-plane shear mode) and mode III (out-of-plane shear mode).

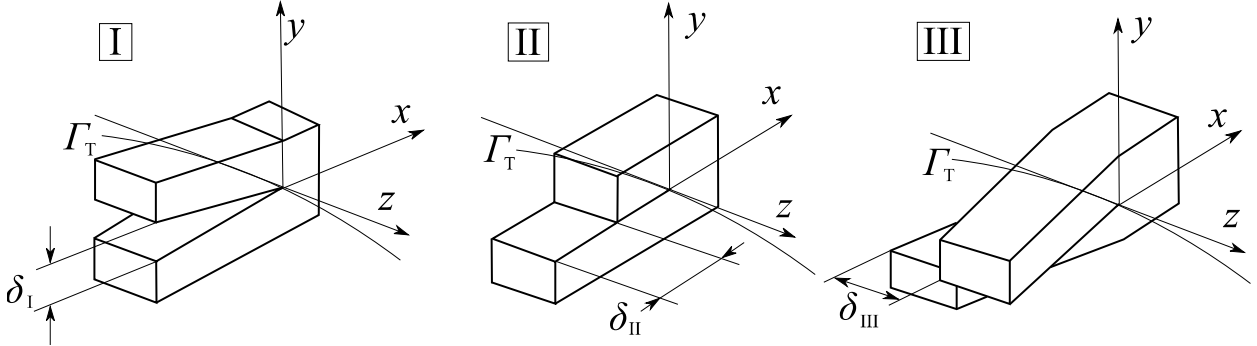


Fig. 1: Loading modes

If the crack front is curved, the three-dimensional character must be taken into account. The stress state varies along the crack front and, in general, it is composed of the fields corresponding to the three crack opening modes. The real-like crack can be solved by superposition of these three modes (Fig. 1). Mode I represents pure normal loading of the crack (opening) and modes II and III are related to pure shear loading. It was proved that fractures in objects propagate mainly in mode I and even if the crack is originally loaded by pure shear mode the propagation tends to divert to normal mode I loading [9]. This means that historically the mode I crack behavior and the mode I propagation is well known [5] while the shear modes II and III are subjected to less research.

There are several approaches to describe the stress and strain fields around the crack tip.

The first one is the K -conception where the main crack parameters are the stress intensity factors (SIFs) – K_I , K_{II} and K_{III} for loading modes I, II and III respectively. The SIF determines a stress singularity at the crack tip and can be expressed in separate form for each loading mode [10] and in these forms it is commonly used for calculations in the field of linear-elastic fracture mechanics:

$$K_i(\sigma, a, L_i) = \sigma \sqrt{\pi a} \cdot k_{cal}(a, L_i); \quad i = I, II, III. \quad (1)$$

Described stress intensity factor is defined by the stress σ in the body with fracture, by the length of crack a and by the calibration function k_{cal} which is related to length of crack a and to the characteristic geometrical dimension L_i of cracked body.

The second commonly used method in the fracture mechanics is an energetic approach developed by Irwin [2, 3]. This approach is based on the energy balance of the system consisting of fractured body and external forces described by the elastic energy of fractured body W_e and the potential energy or work of external forces W_p . Their combination forms energy of the entire system W_c .

With these energies in mind Irwin established a crack driving force G as a change of the energy of system W_c in dependence on the change of crack length a [11]:

$$G = \frac{dW_c}{da}. \quad (2)$$

The relation between energetic approach and the K -conception (under the assumption of the linear-elastic fracture mechanic conditions) can be given by [11]:

$$G = \frac{K_I^2}{E'} + \frac{K_{II}^2}{E'} + \frac{K_{III}^2}{2E_{\text{shear}}}, \quad (3)$$

where E' equals Young's modulus E for plane stress conditions and $E' = E/(1-\mu^2)$ for plane strain conditions (μ stands for Poisson's ratio) and E_{shear} is the shear modulus.

The third commonly used conception in the field of fracture mechanics is the J -integral conception. It is widely used for modeling and calculations under both linear-elastic and elastic-plastic conditions which can occur when materials with low value of yield strength are used [9]. For example, the K -conception cannot be used under such conditions.

The J -integral itself can be expressed (for a simplified 2D model) as [9]:

$$J = \int_{\Gamma} \left(w dy - T_i \frac{\partial u_i}{\partial x} ds \right), \quad (4)$$

$$w = \int_0^{\varepsilon_{ij}} \sigma_{ij} d\varepsilon_{ij},$$

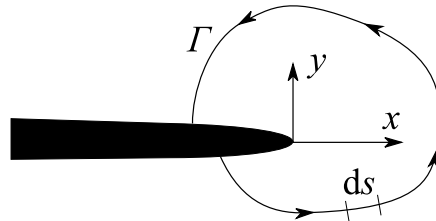


Fig. 2: The crack integration path (2D example)

where T_i are components of the vector of surface forces in perpendicular direction to the integration path Γ , u_i are the components of a vector of relative displacements, s stands for the length of integration path and w is the strain energy density (σ_{ij} and ε_{ij} are the stress and strain tensor components).

Despite the different methods to obtain the crack driving force G and the J -integral, their final values equal and thus (if the linear-elastic fracture mechanics conditions are met) to recalculate the J -integral to SIFs (and vice versa) the same formula (3) as for the crack driving force G can be used.

2.1 INFLUENCE OF THE CRACK MICROSTRUCTURE ON THE FRACTURE PARAMETERS

Material characteristics related to the fracture mechanics are derived from experimental results, but the data evaluation is based on elementary theory for homogenous body with straight planar crack. This theory generally does not account for microstructural patterns of the crack front and flanks. Contrary to this fact, even if the specimen is loaded by the pure remote mode loading the real tortuous shape of crack front leads to decrease of the crack driving force caused by localized mixed-mode I+II+III loading [12, 13].

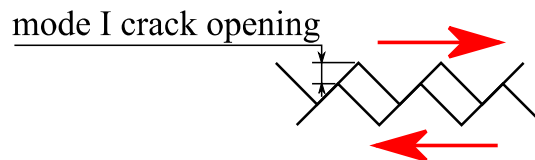


Fig. 3: Example of zig-zag shaped crack under remote mode III loading

Influence of the crack roughness on changes of the crack driving force is called roughness induced shielding (RIS) [14] and it can be seen from various points of view. During the last decades, there have been some works submitting and solving 2D models of RIS [15–19] but these models were far from explaining the real implications of RIS on the fracture behavior even for simple normal loading.

The RIS can be observed from three points of view. The first one was the most investigated in past years and it is related to the crack faces interaction. When remote mode III loading is present, the crack faces slide on each other. If no remote mode I is present and crack faces are assumed to be planar, no crack faces interaction is present. However, real-like cracks are rough and some mode I loading is almost always present in the real applications due to interactions of the crack flanks asperities (see e.g. [20–22] and Fig. 3).

The second one is related to the linear crack front roughness where a zig-zag crack front shape (either simplified or not) is assumed, but the crack front geometrically stays in plane of fracture. It was proved that for serrated cracks under the remote mode III loading there are present local mode II advances of the crack front [23] and thus the crack front geometry has some significant impact on the crack propagation.

In the third approach a full 3D crack model has to be employed to model the crack where small, separate portions of the crack are assumed to be kinked in a 3-dimensional space. The crack kink angle is not uniform along the whole width of the crack, it is changing instead, and it represents a very real-like model of the crack after some propagation. In the year 2003 a statistical approach to this type of crack was introduced [14] for remote mode I loading. This approach accounted for statistical appearance of the fracture roughness and employed a method for quantitative interpretation of some phenomena related to RIS in metallic materials with use of “pyramidal model” of intergranular crack front solved analytically and numerically.

3 AIMS OF THE THESIS

There is some research accounting for the crack front and flanks microstructure, but the knowledge aimed on the fracture mechanics specialized in effects caused by small structural deviances from ideal shape is poor, especially in the field of remote shear mode loading. Even if some simplifications are taken into consideration, the most of existing studies are aimed only on the basic configurations and normal mode I loading [14]. This work aims to contribute to present research on shear loaded fractures affected by deviances from standardized and long used models. Tracked and investigated deviances are mainly the geometrical abnormalities of the fracture geometry from generally used planar models of the crack.

These variances of the fracture surfaces exhibit in different forms for almost all fracture mechanisms. They are mainly governed by the grain structure and microstructural composition of real materials, such as polycrystalline metallic materials. As was mentioned above, these geometrical nuances are mostly deemed as insignificant and their influence is not evaluated. However, if the complex crack shape should be modeled more realistically, the microstructure could be viewed from several different angles.

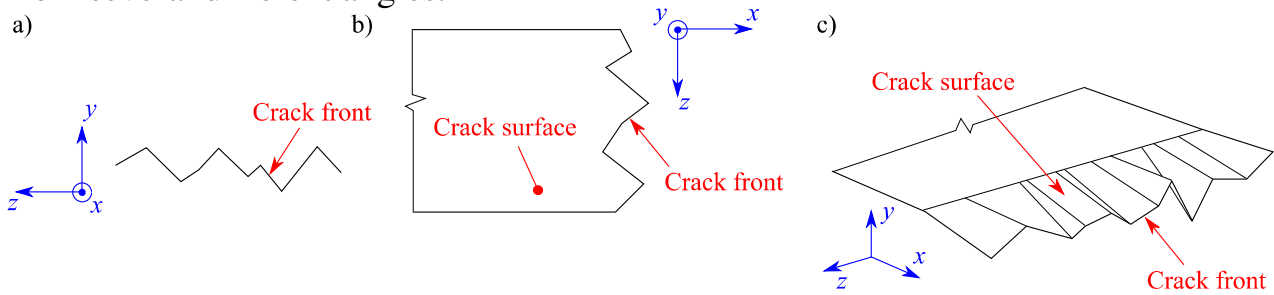


Fig. 4: Schematic examples of the crack microstructure with: a) out-of-plane tortuosity, b) in-plane tortuosity, c) partial tortuosity with twist and kink of the crack

Some examples of the crack micro-geometries are shown in Fig. 4 where all three examples are cracks where the x -axis denotes the general crack propagation direction and the x - z plane is the general crack plane. Schema a) shows the crack with only out-of-plane tortuosity where the crack plane is rough along its whole length, but the crack front lies still in one plane parallel to the y - z plane, schema b) shows in-plane tortuosity where the crack flanks are ideally planar and only the crack front shows tortuosity, but still in the plane x - z , schematic c) then shows partially rough crack with both kink and twist of the crack. In case c) the crack front can lie in one plane the same as in schema a), but it can also introduce some crack front tortuosity like in the schema b). Of course, the combination of cases a) and b) can be modeled too and it is closer to reality than the separate cases.

The crack geometries described in the paragraph above can lead to local induction of all loading modes I, II and III and their combination I+II+III along the crack front which affects resulting crack behavior e.g. during the experimental measurement.

Research in this thesis deals with investigation of influence of the fracture microstructure on SIFs for cracks subjected to the shear mode loading. The aim is to find the relation between the crack front or the crack flanks roughness and fracture parameters. This relation should be investigated for remote mode II and III loading. Investigation of these cases should bring some insight to shear modes behavior therefore this thesis will contribute to broadening of the fracture mechanics theory.

Alongside the investigation of influence of the crack front micro-geometry on the fracture parameters some innovative approaches of evaluation of SIFs along geometrically complex fractures should be created. With use of both analytical and numerical (FEM) approaches, new (more universal) mathematical models should be created if possible. This means both pure mode II and III loading and also mixed-mode II+III loading.

Some correlation between presented models and experimental results is also expected. The findings obtained from numerical and analytical modelling should be used to correct the experimental data in terms of accounting for the crack micro-geometry. Moreover, the results should be compared to the research done by different authors.

4 USED METHODS AND MODELS

In presented dissertation thesis two types of real specimens were investigated in detail – the cylindrical specimen (see e.g. [24–26]) and the compact-tension-shear (CTS) specimen (see e.g. [27, 28]).

At first, the influence of the crack front zig-zag shape in plane of fracture is discussed and some model simplifications are suggested. For this purpose, the cylindrical specimen was modeled, and some results were used in conjunction with the experimental work of Vojtek et al. [8], performed the same specimen.

The second part of this work aims at the decrease of the SIFs due to the crack front and flanks roughness for the remote mode II loading. The CTS specimen is suitable to model this type of the crack roughness (for mode II shear loading). The crack geometry was modeled to resemble the crack surfaces observed on real fractures (either with use of in-plane and out-of-plane roughness or with crack front kink and twist, see Fig. 4). Decrease of calculated SIFs was used for correction of the experimental threshold values which were then compared to the theoretical ones predicted by multiscale models.

For the evaluation of SIFs, the Ansys numerical FEM software was used and all presented variations of models were created in the mentioned program.

4.1 CYLINDRICAL SPECIMEN

The cylindrical specimen can be used for two types of experimental setups – torsion and shear loading. For both setups the same geometry of specimen can be used – a cylindrical bar with circumferential notch. The crack itself propagates from the tip of the notch.

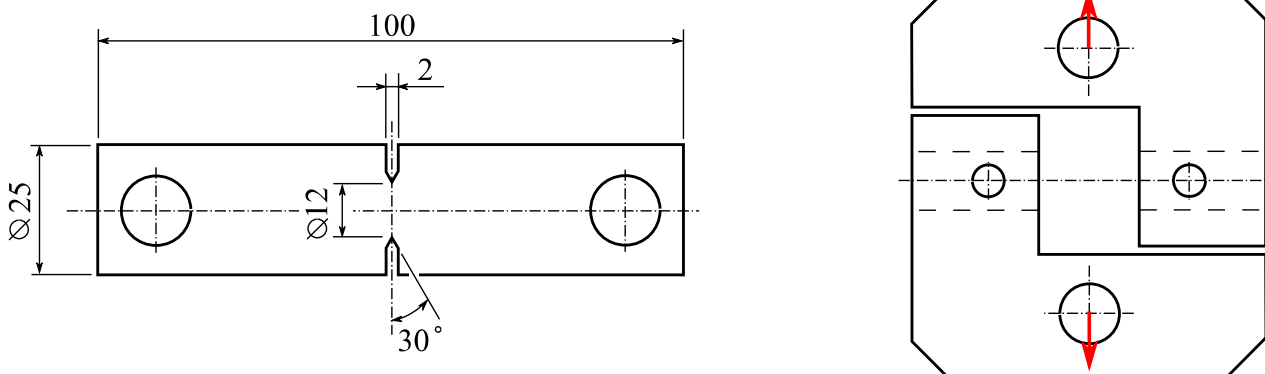


Fig. 5: Schema of the cylindrical specimen (example dimensions) on the left and the loading device (in different scale) on the right

For pure remote mode III loading a torsion loading of cylindrical specimen is ideal. For pure torsion loading the specimen (Fig. 5 left) was clamped in a special device which transforms push-pull loading into torsion momentum [26].

To test pure remote mode II and III and also mixed-mode II+III loading on one specimen simultaneously a special testing device had to be utilized [24, 25]. The gripping device (Fig. 5 right) can be easily mounted in a push-pull device to transform tensile forces to simple shear loading. The specimen itself is clamped

in the central location of the device which assures that at the central point (where the notch with the crack is present) the bending momentum is exactly zero, therefore no superimposed mode I is present.

Actual distribution of modes II and III loading at the crack front around the specimen changes from pure mode II loading to pure mode III loading.

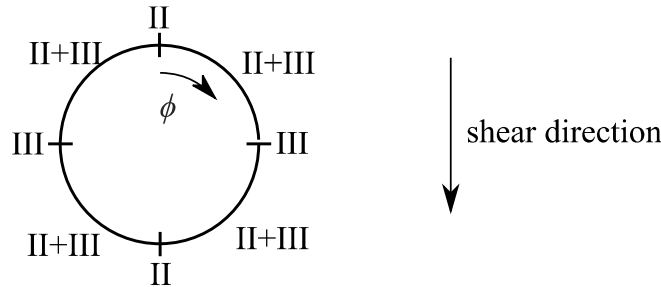


Fig. 6: The specimen cross-section with the corresponding loading modes

At the top and bottom of the specimen a pure mode II loading is present, at sides of the specimen a pure mode III loading is present and between these special points a mixed-mode II+III loading is present (Fig. 6). Loading components are functions of polar coordinate ϕ . Our previous research showed that for coordinate system with $\phi = 0^\circ$ at the top of the specimen the mode II and III SIFs follow functions $\cos(\phi)$ and $\sin(\phi)$ respectively [29].

4.2 CTS SPECIMEN

The CTS specimen was developed for investigation of the cracks loaded by pure mode II and mixed-mode I+II loading. The specimen was created with several requirements in mind [27]: the specimen has simple and compact shape, pure shear mode loading is distributed over large area of the specimen, the crack tip is loaded only by a pure shear mode and the stress conditions are little affected by global geometric alterations.

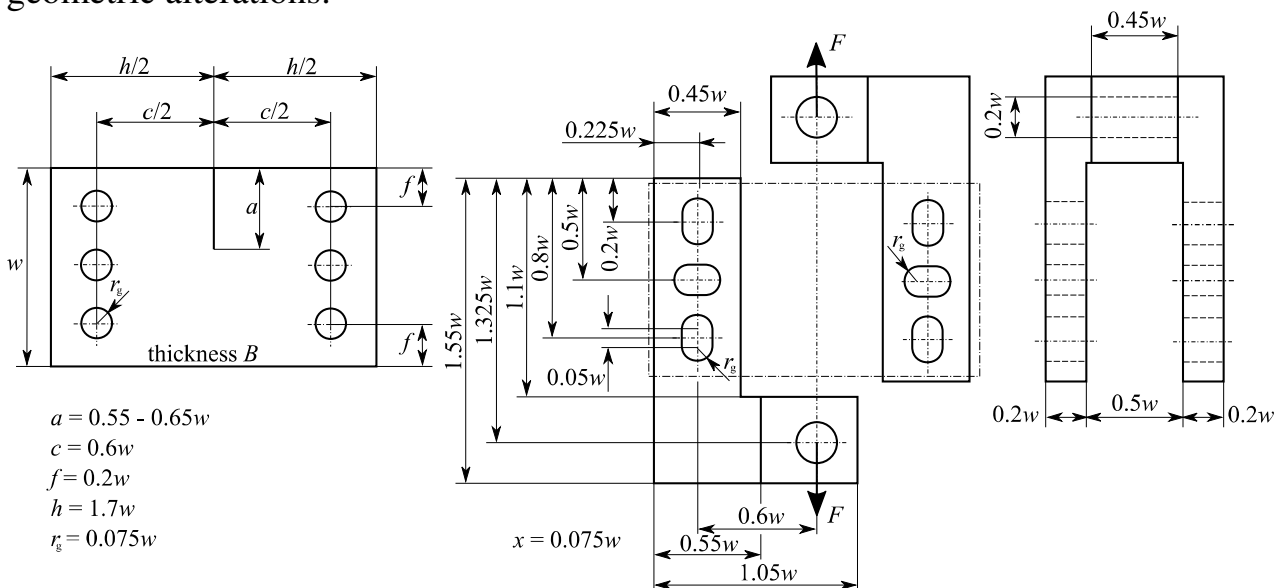


Fig. 7: Original CTS specimen specifications [27]

Richard used the equation for analytical calculation of the SIF K_{II} for original CTS specimen with relative dimensions [27] (which was later rearranged by Plank and Kuhn [28]) from where the K_{II} can be derived:

$$K_{II} = \frac{F}{B} \sqrt{\pi a} \cdot (w-a)^{-1} \left[\frac{-0.23 + 1.4 \cdot \frac{a}{w-a}}{1 - 0.67 \frac{a}{w-a} + 2.08 \left(\frac{a}{w-a} \right)^2} \right]^{\frac{1}{2}}, \quad (5)$$

where F is the applied force, B is the thickness of the specimen and a and w are the characteristic dimensions of the specimen (see Fig. 7).

Richard and Benitz [30] later improved and furthermore investigated this type of specimen and they also adjusted the loading device for mixed-mode I+II loading.

4.3 FE MODELLING

For both types of models (the CTS and cylindrical specimens) the FE model was created with use of submodelling technique [31]. At first the global models of both specimens were created according to the geometries of real specimens (see Fig. 5 and Fig. 7). Each specimen was loaded to model the real loading regimens to mimic shear modes II, III and II+III loading at the crack tip which was modeled smooth without any asperity at this stage of modelling. As a material model used for FE calculations only linear-elastic material properties were considered, and actual values of elastic moduli and Poisson's ratios were used to model the behavior of pure ARMCO iron and niobium according to real experiments done by Vojtek et al. (e.g. [8, 23, 25]), the loading of the specimens was applied at the magnitudes following the same real experiments. In the end, neither of those parameters matter because the SIFs are independent on elastic material properties and all results were normalized to used loading.

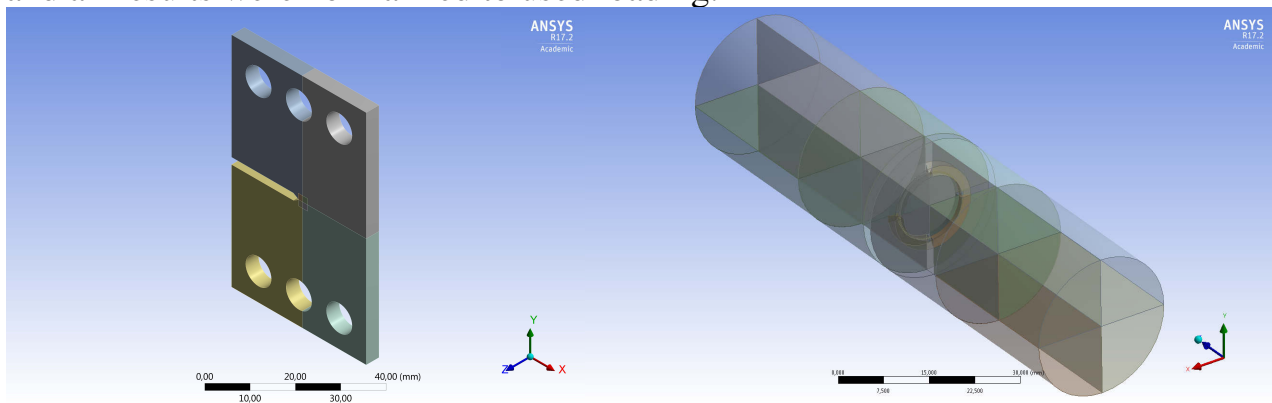


Fig. 8: The examples of global model geometries (CTS specimen on the left and the cylindrical specimen on the right)

For the submodels of the specimens a small portion of geometry of each specimen around the crack was cut out and modelled with very fine FE mesh for a better stress and strain results. Moreover, the crack front and flanks asperities were introduced in this stage of modelling to create desired crack front and flanks microstructure.

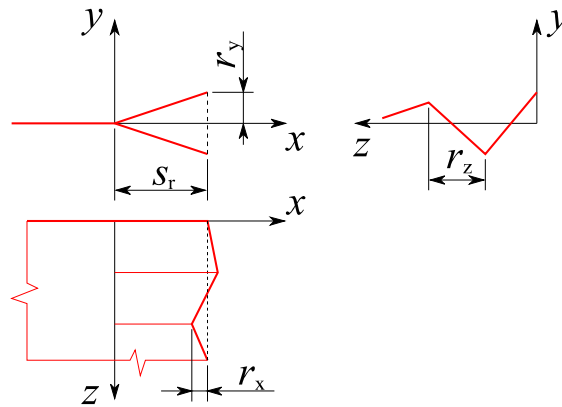


Fig. 9: Schematic of tortuous crack front and flanks (red line denotes the crack)

According to the schematic in Fig. 9 the crack front and flanks tortuosity in used models could be controlled by four geometrical parameters – the length of tortuous portion of crack s_r and the amplitude of crack front roughness in each of 3D directions r_x , r_y and r_z . If the parameter s was used, it was set as a constant along the whole crack front. On the other hand, the roughness parameters were used in a more complex way. To suit the needs of each model, any of the three r -parameters could be set as a constant (usually with alternating \pm symbol), at a zero value or it could be used only as the amplitude which was multiplied by a random number in range from -1 to 1. This randomization was used in the advanced models to create random pattern of crack front and flanks asperities and by this way to model the most real-like crack. To enable full control and repeatability of the model this randomization was governed by a key parameter. If two models with the same key parameter were created, the random pattern of these models was the same.

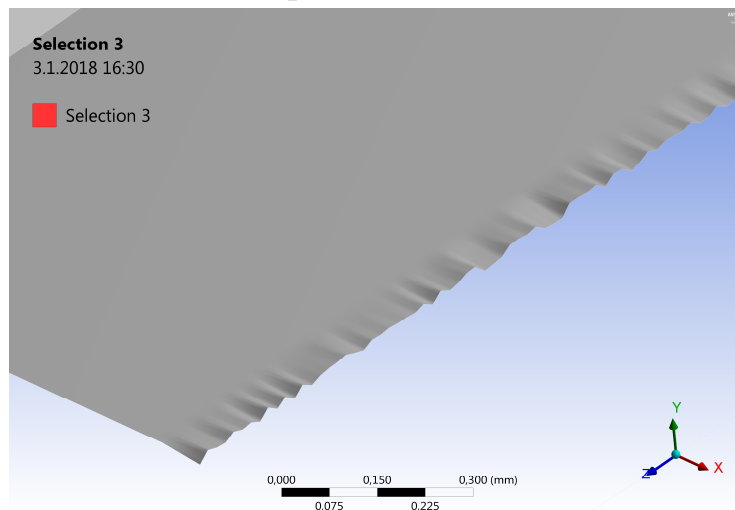


Fig. 10: Example of the rough crack front and flanks with use of all roughness parameters

Along the tortuous crack front the SIFs were calculated using Ansys built-in subroutine CINT which calculates in each mesh node the values of SIFs with use of contour integration [31].

5 RESULTS

The cylindrical specimen crack front roughness was considered to be only in-plane, and it was decided that only uniform crack front asperities will be included in this type of model. Within the frame of these constrictions, two types of models were investigated. The first one aimed at description of simplification possibilities of the crack front roughness and the second one was aimed at the investigation of the influence of crack front microstructure on crack propagation during shear mode loading.

Unlike the cylindrical specimen, for the CTS specimen there were more researched variants. In general, two observation methods were used – local view on local k_1 , k_2 and k_3 along one distinct crack front asperity and a description of influence of crack roughness on the mean progression of the SIFs along the crack front.

5.1 MODEL SIMPLIFICATIONS (CYLINDRICAL SPECIMEN)

Besides standard steps for efficient modelling (for example submodelling, efficient FE mesh sizing etc.) a geometry simplification was considered while modelling the cylindrical specimen. The simplification in terms of modelling only one particular part of crack front (area of interest) with geometrical asperities was considered and the rest of the crack front could be simplified.

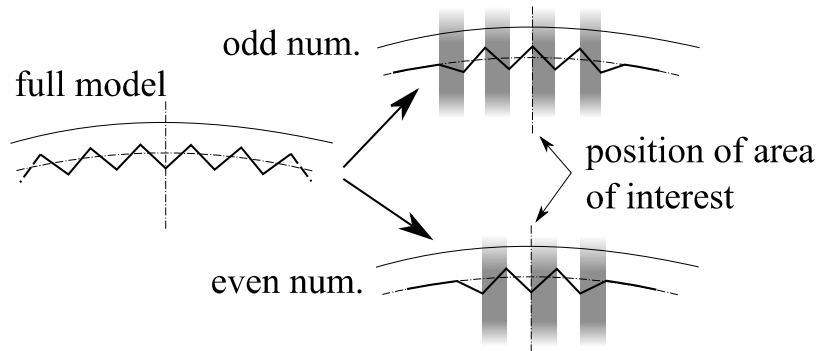


Fig. 11: Example of the crack front simplification system

The difference between full and simplified models can be seen in Fig. 11 where two types of simplified models are shown. Since the number of modeled teeth around the area of interest was one variable for modelling and the symmetry of the model was needed to be preserved the simplified model had to be divided into two groups – one with odd number of teeth and the second with even number of teeth. Each simplified model was compared with corresponding full model with the same characteristic dimensions of teeth. Observed value was the relative difference of the local SIFs between the full model and simplified model ($k_{i, \text{full}}$ and $k_{i, \text{simple}}$ respectively, where $i = 2$ or 3) at each location around the specimen denoted by the angular coordinate ϕ (see Fig. 6):

$$\delta k_i = \frac{|k_{i, \text{full}}(\phi) - k_{i, \text{simple}}(\phi)|}{k_{i, \text{full}}(\phi)} \cdot 100\%. \quad (6)$$

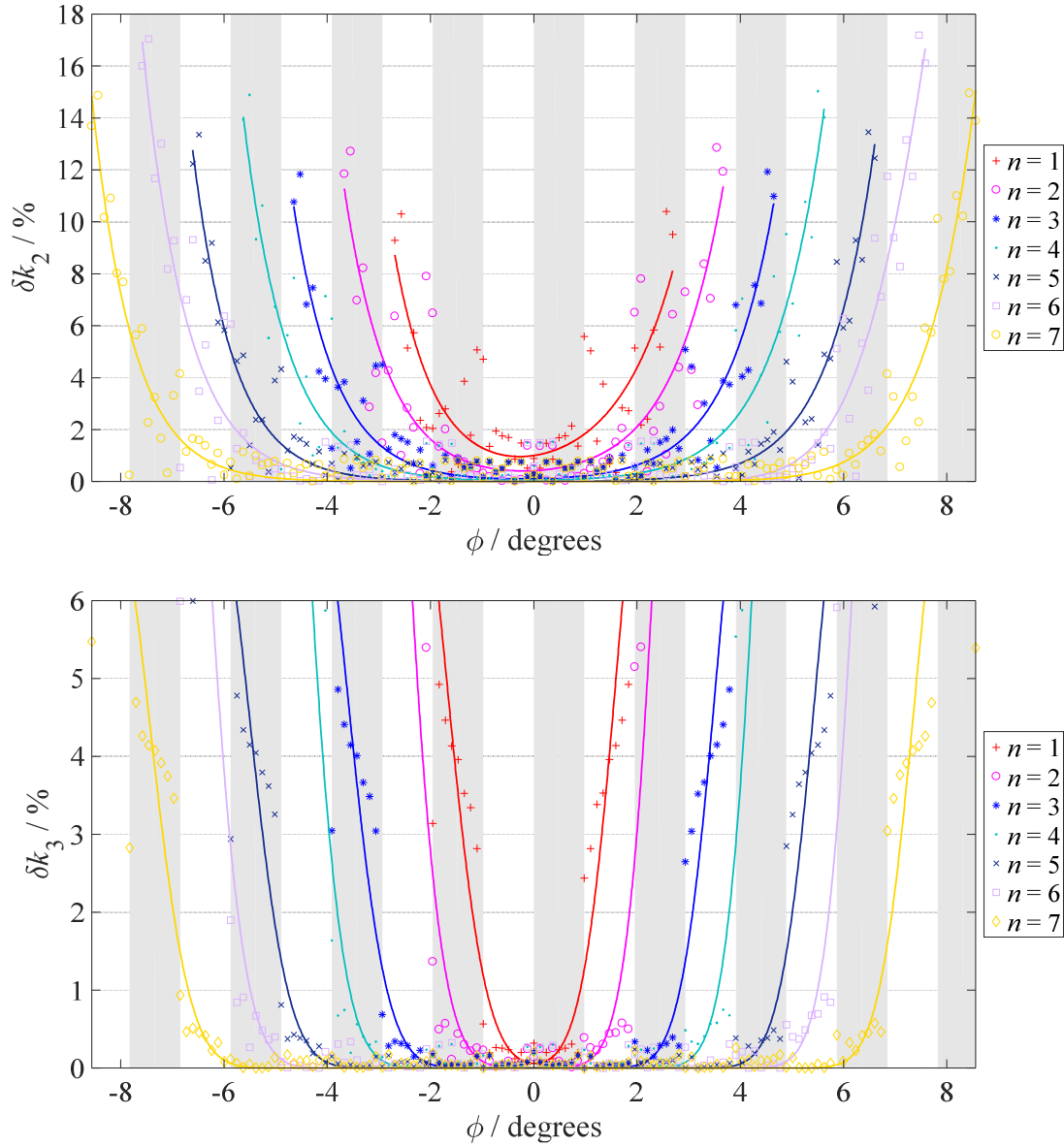


Fig. 12: Example of δk_2 (upper chart) and δk_3 (lower chart) at position $\phi = 0^\circ$

Resulting differences (example) according to Eq. (6) are shown in Fig. 12 where several numbers of teeth n were plotted, and each white and gray strip represents one half-tooth. Closer look on results for $n > 2$ suggests that core teeth (for example for $n = 4$ core teeth are the second and the third ones etc.) give very accurate, almost identical results as full model and the side teeth facets and the transition facets show difference increasing with the distance from center of the area of interest. Obtained results confirm that, for the investigated types of serrated crack fronts and loading, the local SIFs are influenced only by the close surroundings of investigated area. The lowest undisrupted area corresponds to that in between the two regular teeth framed on sides by the transition asperities, excluding these two side teeth – the lowest n should be 3 for case where only one tooth is investigated.

Full results set was already published by the author of these thesis topics in a paper [32].

5.2 MODE III CRACK PROPAGATION (CYLYNDRICAL SPECIMEN)

Description of micro-mechanisms of crack propagation under remote mode III loading is rather difficult. There have been some attempts to describe this type of crack propagation qualitatively (by observation of fractographical patterns) and it was deduced that serrated crack front under remote mode III loading exhibits local mode II crack propagation due to geometrically induced local mode II loading [33]. To confirm and help quantify this phenomenon the cylindrical specimen with a zig-zag crack front was modeled (similarly to the model in chapter 5.1, with adjustable asperity angles) and local SIFs values were obtained along each serration. Modeled teeth angles ranged from 3.35° to 41.65° .

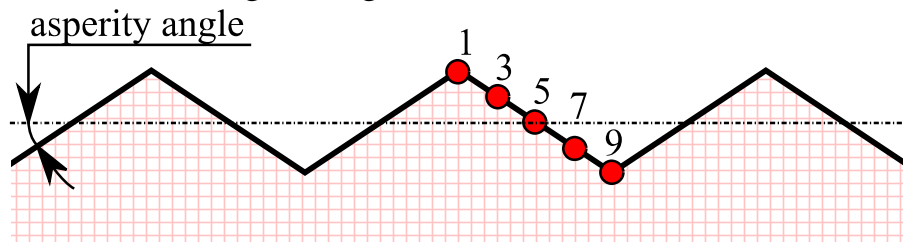


Fig. 13: Positions and numbering of evaluation nodes along the crack front serration (only odd numbers are shown) and the asperity angle schematic

Actual observed results were at location of remote mode III loading at one crack front tooth facet. On one facet there were 9 evaluation nodes to obtain local SIFs (see Fig. 13 area with red lines pattern represents un-cracked material and area above zig-zag line represents crack faces). Simulation was calculated for two material models (ARMCO iron and niobium according to experiments by Vojtek et al., e.g. [8, 23, 25], see chapter 4.3) to compare the results with experimental data.

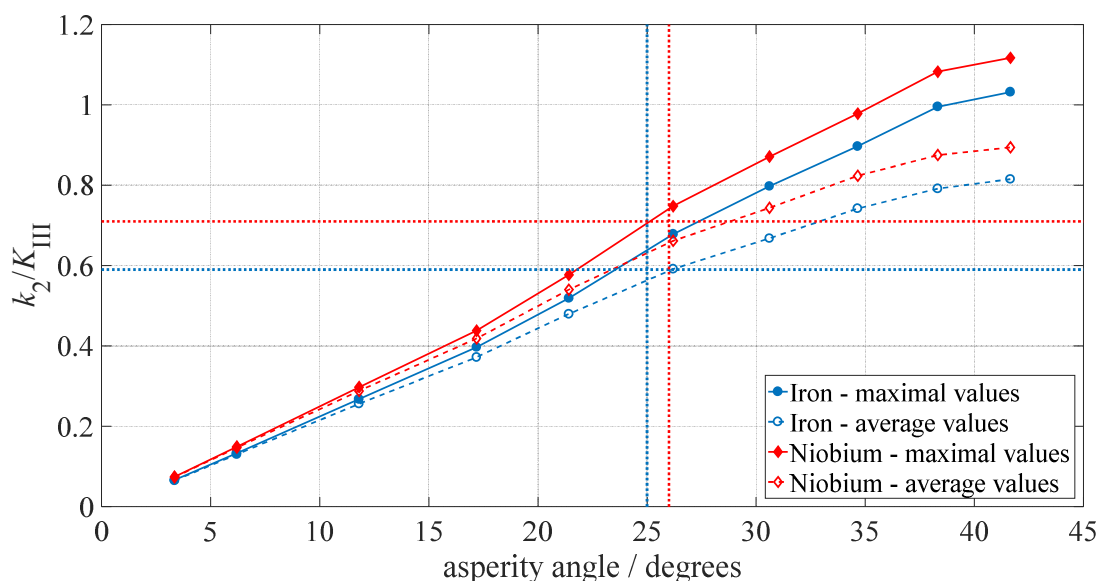


Fig. 14: Resulting ratio k_2/K_{III} for different asperity angles and two material models

As a result for comparison local mode II loading with global remote mode III loading, a ratio of locally induced k_2 values to global K_{III} were obtained along the crack front serration. Because resulting ratios were not constant along the crack asperity (they were decreasing with maximum at the node No. 2), the maximal and averaged values were used for evaluation. Results for evaluated asperity angles can be seen in Fig. 14 together with experimentally measured results – the crossing points of dotted lines (with respective colors for each material) represent intersection of experimentally measured threshold ratios $\Delta k_{2,eff th}/\Delta K_{III,eff th}$ and mean asperity angles for used materials obtained from fractography. Measured ratios of effective mode II and mode III thresholds and mean asperity angles are 0.59 and 25° respectively for iron and 0.71 and 26° respectively for niobium [23, 32, 33].

Comparison of experimentally measured angles and effective threshold ratios with numerical models shows a very good agreement. It showed that even with relatively small asperity angles at the in-plane pre-crack front the local induced mode II loading (and hence mode II crack propagation mechanisms) can contribute to propagation of crack under remote mode III loading. Therefore, this numerical model helped with quantitative description of mode III crack propagation assisted by mode II mechanism. These findings and their implications were published by the author of these thesis topics (and his colleagues) in [8, 36].

5.3 UNIFORM CRACK ROUGHNESS (CTS SPECIMEN)

As was described in previous chapters, the crack front and flanks geometry is planar in minimum of real-life cases. In fact, the observations of the cracks and pre-cracks morphology showed significant in-plane and out-of-plane roughness of the crack geometry [6, 37]. Small changes in the crack front and flanks micro-geometry affects overall SIFs progressions along the crack front. For this case, a uniform distribution of the crack front asperities along the fracture in CTS specimen loaded in pure remote mode II were investigated.

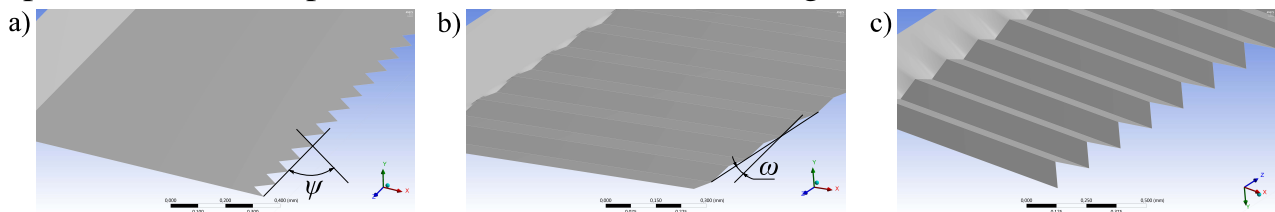


Fig. 15: Example of: a) in-plane, b) out-of-plane crack front roughness and c) combination of previous cases

The crack micro-geometry was modeled in three different types. At first, the in-plane tortuosity was modeled (Fig. 15 a)) where the crack front followed the zig-zag shaped path but the crack itself with crack front stayed in the x - z plane. Each crack tooth was described by angle ψ which was the same for all teeth along the crack front and varied from 11.2° to 43.6°. The second investigated type of crack front tortuosity was out-of-plane roughness (Fig. 15 b)) characterized by the zig-zag morphology only in the y - z plane (factory-roof-like morphology) with all asperities characterized by angle ω which varied from 14.0° to 26.6°. The third configuration

of modeled crack geometry was the combination of two previous cases (Fig. 15 c)) characterized by both asperity angles. The range of angles ψ and ω was chosen to correspond with the naturally occurring range of crack front and flanks roughnesses.

Local changes of SIFs along the crack front caused by different types of modeled crack micro-geometries showed that, in the case of in-plane tortuosity, the component k_1 exhibits only very small local oscillations with zero mean value along the whole crack front, i.e. it practically does not differ from that for the straight crack front. The components k_2 and k_3 oscillate with much higher amplitudes and their mean values also change along the crack front which represents a rather significant difference comparing to the results for the straight crack front.

In the case of the out-of-plane roughness, the local k_1 -values were more pronounced particularly at the crack front points adjacent to free surfaces (specimen sides). On the contrary, the values of k_2 and k_3 components were almost unaffected and coincided with those for the straight front. The combination of both types of roughnesses showed differences of all three local SIFs from those of the planar (straight) crack, but slightly less significant when compared to the previous types.

For the assessment of the local SIFs, each crack asperity along the crack front was modeled to have nine evaluation nodes along one half-tooth from which the first and the last one was shared by the previous or the next asperity (in the same way as was constructed model of the cylindrical specimen, see Fig. 13). This means that for each elementary crack front serration nine evaluation points for obtaining the local SIFs were available but the first and the last one had to be omitted, since the crack front direction could not be well defined there. Therefore, in the further description of the results only the nodes No. 2 – 8 will be utilized, where the ratios of the local k_3 and k_1 SIFs to remote mode II SIF K_{II} were evaluated for in-plane and out-of-plane roughness, respectively, and for all selected values of the angles ψ and ω [38].

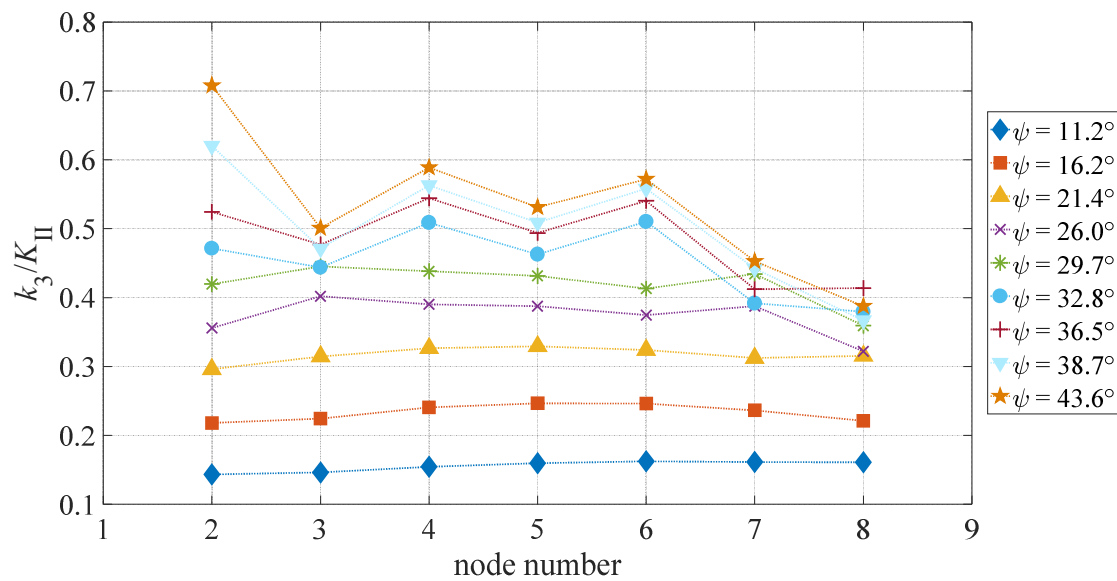


Fig. 16: Normalized values of local k_3 along one crack asperity (in-plane roughness)

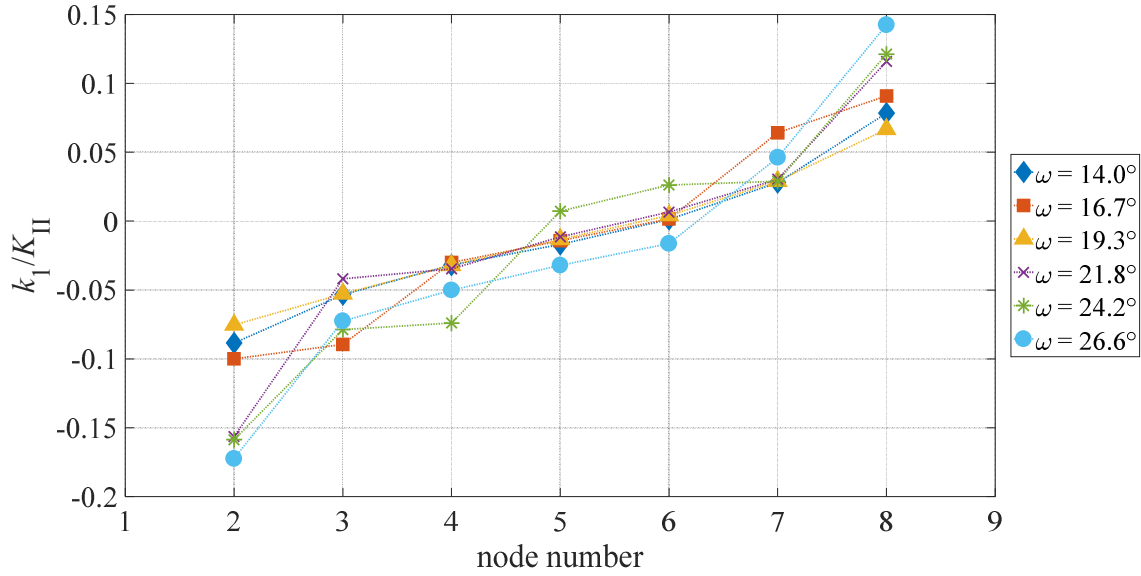


Fig. 17: Normalized values of local k_1 along one crack asperity (out-of-plane roughness)

The local values of the ratio k_3/K_{II} along the half-tooth show an expected increase with an increasing angle ψ for the in-plane roughness (Fig. 16). In addition, the ratios k_3/K_{II} for ψ higher than 26.0° tend to exhibit an increase towards the evaluation node No. 2, which is more pronounced for the highest asperity angle 43.6° . This node lies at the innermost part of the crack tooth where the crack length is the smallest, but the stress concentration is the highest due to the effect of the asperity [38]. The increase of the local mode III SIF towards the node No. 2 is in a qualitative agreement with the results for the local k_2 obtained for a serrated crack front loaded by remote mode III, which were described similarly in terms of the ratio k_2/K_{III} in chapter 5.2 where the cylindrical specimen was examined.

On the other hand, the ratio k_1/K_{II} for cracks with out-of-plane roughness (Fig. 17) is very small. This ratio should be even zero along the entire out-of-plane tooth according to a simple stress tensor transformation method. It means that the small tensile and compressive stresses are just local perturbations resulting from a more accurate numerical analysis describing the full complexity of the 3D model [38].

From the global point of view the change of mean functional values of SIFs from rough cracks was visible in all investigated cases. This change can be described by quotient Q_i which represents the change in the functional mean value of the results. Mentioned quotient can be defined as follows - if the set of result points of the local SIFs from the model with the rough crack front is interpolated by a function which is a Q_i -multiple of function $K_{i,n}(z)$ (the functional description of results for the standard simple straight crack), the coefficient Q_i actually quantifies the ratio between (a sort of) mean value of results from rough crack and results from planar model of crack and thus it describes the decrease of global SIF value. Only the mode I SIF was omitted from evaluation of Q_i , because in all cases k_1 oscillates around the $0 \text{ MPa}\cdot\text{mm}^{1/2}$, hence the quotient Q_i would be nonsensical.

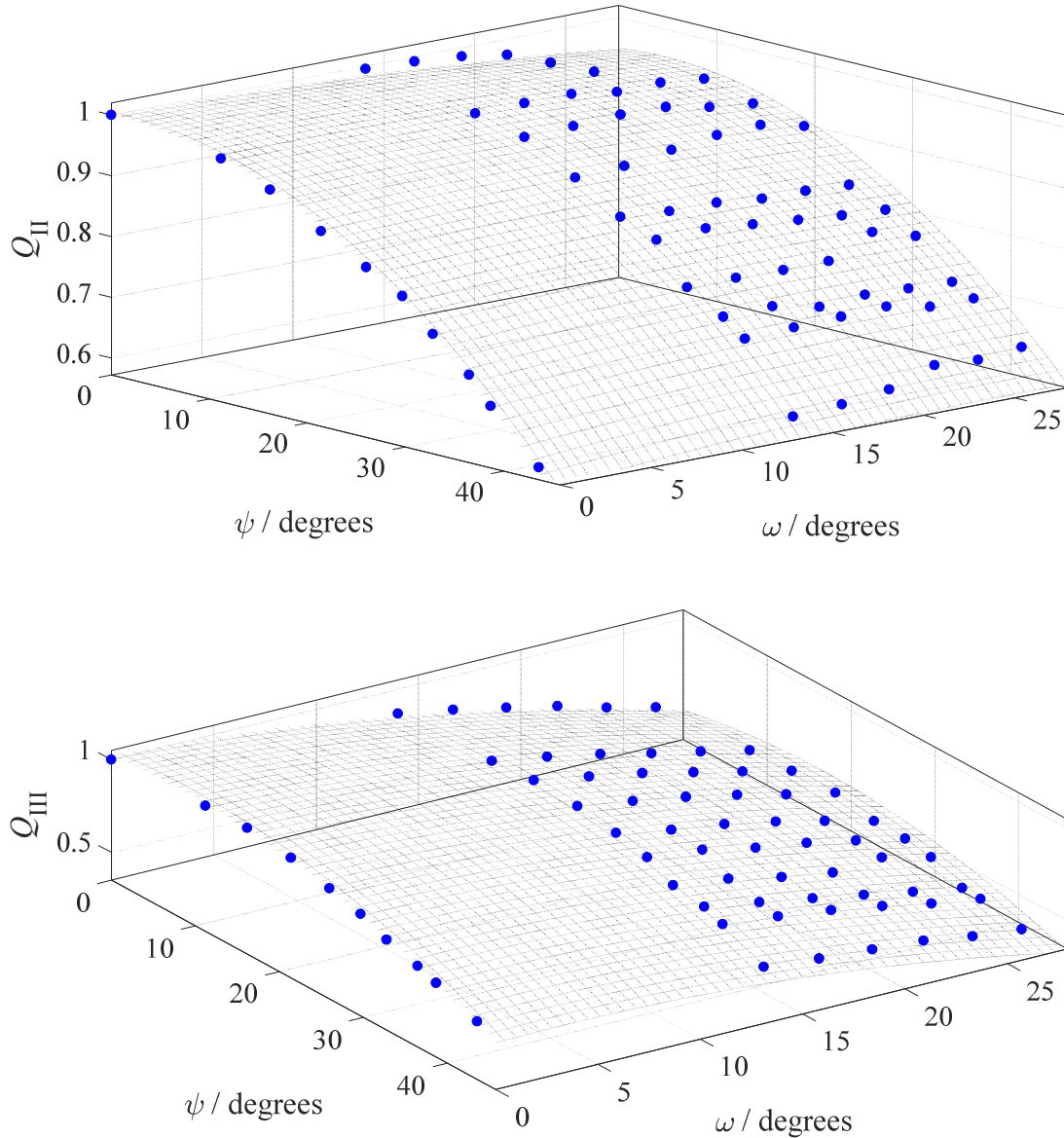


Fig. 18: Quotient Q_{III} as a function of both asperity angles ψ and ω

Quantified quotients Q_{II} and Q_{III} as functions of angles ψ and ω are visible in the Fig. 18. Obviously, both mode II and III SIFs at the rough crack front are decreasing with increasing angles ψ and ω (increasing roughness) due to the geometrical shielding effect. The decrease of mode II SIF values is much more influenced by the in-plane tortuosity than by the out-of-plane roughness, while the mode III SIF values decrease more rapidly and in a similar rate for both ψ and ω angles. The results obtained for global SIFs can be utilized to correct experimental values of mode II effective fatigue thresholds in metallic materials obtained under the assumption of smooth pre-crack. According to Fig. 18, for example, the reduction of the measured threshold values for ARMCO iron and niobium should be around 15% since the in-plane mean angles of the pre-crack fronts measured in these materials were $\psi = 25^\circ$. However, this correction is just a rough prediction, since no precise observation of real angles ψ and ω was performed.

5.4 TILT AND TWIST OF THE CRACK FRONT (CTS SPECIMEN)

The other type of crack front and flanks tortuosity is the complex 3D crack front tilt and twist. In this case almost whole crack from the notch tip is considered planar, but in the area close to crack front the crack starts to deviate from its planar shape to both upper and bottom directions.

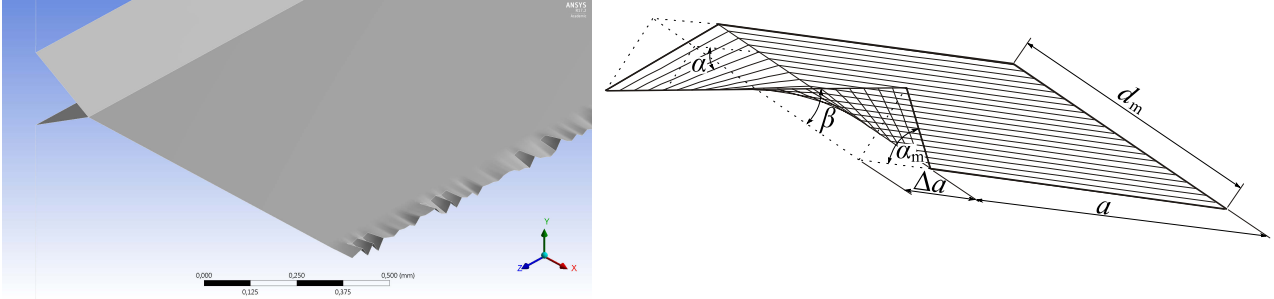


Fig. 19: Examples of modelled twist and tilt of the crack front

Two types of models were considered: the numerical model of the crack with random distribution of the crack front asperities (Fig. 19 left) and an analytical model (Fig. 19 right) containing only one crack front asperity with the width d_m , crack length $a + \Delta a$, changing tilt angle α (with maximal value α_m) and twist angle β . The results from numerical model were described by coefficient Q_{II} (similarly to the previous chapter) and the analytical model could be described by similar ratio:

$$k_2 / K_{II} = \frac{1}{2\alpha_m} \cdot \int_{-\alpha_m}^{\alpha_m} k_2 / K_{II}(\alpha, \beta) d\alpha, \quad (7)$$

where the function $k_2/K_{II}(\alpha, \beta)$ is (with use of simple tensor transformation):

$$k_2 / K_{II}(\alpha, \beta) = \left[1 - \sin\left(\frac{\alpha}{2}\right) \cdot \sin\left(\frac{3\alpha}{2}\right) \right] \cdot \cos\left(\frac{\alpha}{2}\right) \cdot \cos(2\alpha) \cdot \cos(\beta) + \frac{1 + \cos^2(\beta)}{4} \cdot \sin(\alpha) \cdot \sin(2\alpha) \cdot \cos\left(\frac{3\alpha}{2}\right) + \sin\left(\frac{\alpha}{2}\right) \cdot \sin(2\alpha) \cdot [1 - \mu \sin^2(\beta)]. \quad (8)$$

Angles α and β can be related to the linear roughness of the crack front R_L :

$$\alpha_m = \tan^{-1} \left[\frac{d_m \cdot \tan(\beta)}{2\Delta a} \right], \quad (9)$$

$$\beta = \cos^{-1} \left(\frac{1}{R_L} \right).$$

Comparison of these two models was done using two different R_L values (for the random FE model the mean value from several simulations was used).

Table 1: Comparison of the numerical and analytical models

	$R_{L,1} = 1.078$	$R_{L,2} = 1.261$
k_2/K_{II} (analytical model)	0.9270	0.7912
Q_{II} (numerical model)	0.8981	0.7588
Relative deviation between models	3.12 %	4.10 %

There is a good agreement between the analytical and numerical models. Despite the difference in terms of uniform contra statistical distribution of the crack front asperities, the relative deviation between the two averaged ratios is for both crack front roughnesses under 5 % [39]. Moreover, obtained coefficients can be used for correction of the experimentally measured fatigue threshold for ARMCO iron, ($\Delta K_{IIth, \text{eff}} = 1.5 \text{ MPa}\cdot\text{m}^{1/2}$ for $R_{L, \text{Fe}} \approx 1.2$ [40]). With use of obtained quotients, this value can be corrected to $1.2 \text{ MPa}\cdot\text{m}^{1/2}$. This corrected value can be compared to the theoretical SIF related to the emission of dislocations in the cracked iron single crystal, obtained from multiscale quasi-continuum models $K_{IIc} = 0.7 \text{ MPa}\cdot\text{m}^{1/2}$ [41]. With use of correctional factor of 1.3 suggested by Riemelmoser [42], experimentally measured value decreases even to $0.93 \text{ MPa}\cdot\text{m}^{1/2}$, which is closely approaching the theoretical threshold [39].

5.5 FULLY RANDOM CRACK FRONT AND FLANKS GEOMETRY (CTS SPECIMEN)

The last investigated type of crack front tortuosity was combination of kinked/twisted crack with in-plane tortuosity. This particular type of simulation was created to look into the influence of fully random crack front shape. Moreover, two types of material models were used here to check the influence of material parameters (mainly Poisson's ratio set to $\mu = 0.3$ for standard model and $\mu = 0$ for artificial model).

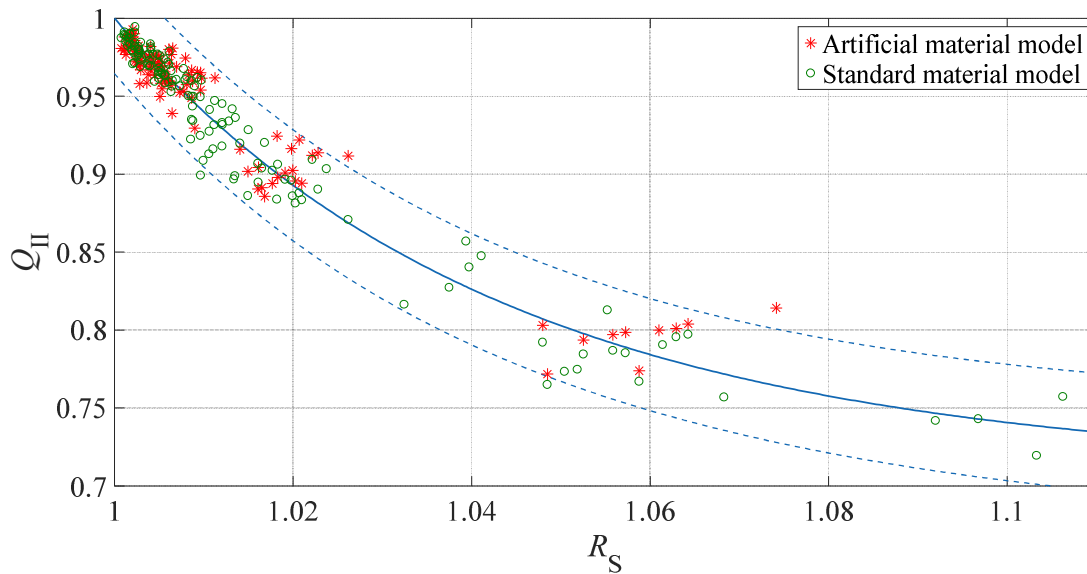


Fig. 20: Coefficient Q_{II} as a function of crack flanks roughness R_S

The evaluation of resulting coefficient Q_{II} as a function of the surface roughness R_S (Fig. 20) of the crack flanks, obtained directly from the FE models showed, that the difference caused by the Poisson's ratio is very small. In the end, all of the results combined were interpolated by a power-law function (with the 99% confidence limit showed as a blue dashed line in Fig. 20) which asymptotically approaches value of $Q_{II, c} \approx 0.7$, thus the smallest coefficient decreasing the applied $K_{II, \text{app}}$ should not be less than 0.7 for this type of tortuous cracks [43].

6 CONCLUSIONS

During the Ph.D. research new modelling approaches were used for a description of fracture behavior of cracks with rough crack flanks and tortuous crack fronts. Several phenomena related to the geometrically induced shielding for shear modes loading were described and some of them were applied in relation to experimental measurement of the fatigue threshold values for metallic materials.

Described research confirmed the influence of the crack front microstructure and extended the knowledge about the geometrical shielding on shear modes where it was not investigated as much as for loading mode I. For this purpose, two types of specimens were investigated – cylindrical specimen and CTS specimen.

Calculations performed on the cylindrical specimen revealed that it is not necessary to model the whole specimen with tortuous crack front, but one can model in detail a very small part of the crack around the place of interest, but in the rest of the model the crack front and flanks can be modeled as a simplified plane without influencing wanted results. In fact, for sufficient accuracy of the resulting SIFs along any asperity on crack front only one or two additional asperities have to be modeled on each side of the region of interest. This finding can help in acceleration of calculations of future models of cracks with the tortuous crack front where only a small portion of actual fracture is investigated.

The second thing related to the cylindrical specimen in this research was actual quantification of the local k_2 influence on crack propagation under remote mode III loading. It was shown that for in-plane zig-zag shaped crack fronts the induced local k_2 along each asperity is strongly dependent on actual asperity angle – mode II inducement increases with higher asperity angles and for angles larger than 15° the induced k_2 is not constant along the whole crack tooth but it increases towards the crack tooth peak. Comparison of numerically modeled ratios of k_2/K_{III} with experimentally measured ratios of the fatigue threshold values for modes II and III showed that modeled ratios of k_2/K_{III} correlates with the threshold values well and thus the local mode II crack advances under remote mode III loading could be quantified for ARMCO iron and Niobium.

For the CTS specimen under the remote mode II loading the influence of several crack front and flanks roughnesses were investigated. Using only numerical FE models a decrease of mean $k_2(z)$ value in comparison with applied $K_{II,app}$ was quantified by quotient Q_{II} for in-plane and out-of-plane crack roughness and also for their combination. This quantification revealed that the in-plane crack front tortuosity has much larger influence on the mode II SIF decrease than the out-of-plane tortuosity. Overall decrease of the mode II SIF can be used to correct experimentally measured values of SIFs if the real crack asperity mean angles are known. The same simulations were used to investigate local modes inducement along one particular asperity. For the in-plane crack front tortuosity qualitatively the same result as for the cylindrical specimen was observed, but with locally induced k_3 in relation to global K_{II} . On the other hand, for the out-of-plane tortuosity, despite no obvious reason, mode I SIF was induced along each particular

crack front asperity. Closer observation of this phenomenon showed that the small amount of induced k_1 can be clarified – small tensile and compressive stresses were just a local perturbation resulting from accurate numerical model and they have no direct connection to the crack front rotation.

The last step in modelling of the complex crack front shape was to create model where only a small portion of crack length is rough, and the rest is planar. This corresponds to experimentally observed crack morphologies where part of a crack was created ultra-fine and planar on purpose but the rest, after some shear crack propagation, exhibited some roughness. For the investigation of this type of shear cracks both numerical and analytical models with combination of crack front kink and twist were introduced. The analytical model included several simplifications, but the numerical model included random crack front shape (governed by mean crack front linear roughness). Comparison of the numerical and analytical approaches led to the conclusion that both methods can describe the decrease of the mean k_2 value very well. In fact, the resulting coefficients Q_{II} were used to correct experimentally measured fatigue threshold value for ARMCO iron (measured under the assumption of straight crack front) and to correlate the threshold value with theoretical multiscale quasi-continuum models. Moreover, overall decrease of the mean values of SIFs for this type of crack front and flanks geometry was quantified and related to crack geometrical shielding effect. One particular part of presented research showed that the decrease of mean value of $k_2(z)$ with increasing crack front and flanks roughness is independent on all linear material properties (despite the fact that the Poisson's ratio influences overall progression of K_{II} and K_{III}).

In conclusion, advances in presented research helped mainly in the path for correction of experimentally measured SIFs to the real crack front microstructure for the remote shear loading. Newly used coefficient Q_i can be used for such correction when the actual crack front and flanks roughness is known. In addition, new models of the shear cracks (statistical approach in FE models and one new analytical model) enable new possibilities in this branch of research. These new models can be used in further research in correlation with more experimental results. Furthermore, the same approach as was used here in FE modelling can be extended for different, more complicated crack flanks geometries and even create models as exact copies of SEM observed crack morphologies.

REFERENCES

- [1] Roylance, D.: Introduction to Fracture Mechanics. 32, 1–17 (2001).
doi: 10.2472/jsms.32.935
- [2] Irwin, G.R., Kies, J.A.: Fracturing and Fracture Dynamics. Weld. J. Res. Suppl. (1952)
- [3] Irwin, G.R., Kies, J.A.: Critical Energy Rate Analysis of Fracture Strength of Large Welded Structures. Weld. J. Res. Suppl. (1954)
- [4] Rice, J.R.: A Path Independent Integral and the Approximate Analysis of Strain Concentration by Notches and Cracks. J. Appl. Mech. 35, 379 (1968).
doi: 10.1115/1.3601206
- [5] Pook, L.P.: A 50-year retrospective review of three-dimensional effects at cracks and sharp notches. Fatigue Fract. Eng. Mater. Struct. 36, 699–723 (2013). doi: 10.1111/ffe.12074
- [6] Vojtek, T., Pokluda, J., Hohenwarter, A., Pippan, R.: Three-dimensional morphology of fracture surfaces generated by modes II and III fatigue loading in ferrite and austenite. Eng. Fract. Mech. 108, 285–293 (2013).
doi: 10.1016/j.engfracmech.2013.02.022
- [7] Vojtek, T., Pokluda, J.: Experimental Investigation of Modes II and III Fatigue Crack Growth in Unalloyed Titanium. Key Eng. Mater. 592–593, 797–800 (2013). doi: 10.4028/www.scientific.net/KEM.592-593.797
- [8] Vojtek, T., Žák, S., Pokluda, J.: On the connection between mode II and mode III effective thresholds in metals. Fract. Struct. Integr. 0, 245–251 (2017).
doi: 10.3221/IGF-ESIS.41.33
- [9] Pokluda, J., Kroupa, F., Obdržálek, L.: Mechanické vlastnosti a struktura pevných látek: kovy – keramika – plasty. 1st edition. PC-DIR spol. s.r.o. - Nakladatelství, Brno (1994). ISBN: 80-214-0575-9
- [10] Irwin, G.R.: Analysis of Stresses and Strains Near the End of a Crack Traversing a Plate. J. Appl. Mech. 24, 361–364 (1957)
- [11] Anderson, T.L.: Fracture mechanics: Fundamentals and applications. CRC Press, Boca Raton (Florida) (1995). ISBN: 9781420058215
- [12] Kobayashi, A.S., Wade, B.G., Bradley, W.B., Chiu, S.T.: Crack branching in Homalite-100 sheets. Eng. Fract. Mech. 6, 81–92 (1974).
doi: 10.1016/0013-7944(74)90048-4
- [13] Kitagawa, H., Yuuki, R., Ohira, T.: Crack-morphological aspects in fracture mechanics. Eng. Fract. Mech. 7, 515–529 (1975).
doi: 10.1016/0013-7944(75)90052-1
- [14] Pokluda, J., Šandera, P., Horníková, J.: Statistical approach to roughness-induced shielding effects. Fatigue Fract. Eng. Mater. Struct. 27, 141–157 (2004). doi: 10.1111/j.1460-2695.2004.00734.x
- [15] Suresh, S., Ritchie, R.O.: A geometric model for fatigue crack closure induced by fracture surface roughness. Metall. Trans. A. 13, 1627–1631 (1982).
doi: 10.1007/BF02644803

- [16] Suresh, S.: *Fatigue of Materials*. 2nd edition. Cambridge University Press (1998). doi: 10.1017/CBO9780511806575
- [17] Llorca, J.: Roughness-induced fatigue crack closure: A numerical study. *Fatigue Fract. Engng. Mater. Struct.* 655–669 (1992). doi: 10.1111/j.1460 2695.1992.tb01304.x)
- [18] Wang, S.H., Muller, C.: Analytical evaluation and experimental study of roughness-induced crack closure. In: Wu, X.R. and Wang, Z.G. (eds.) *Fatigue 99*. pp. 539–544. , Beijing (1999)
- [19] Pokluda, J., Šandera, P., Horníková, J.: Statistical model of roughness-induced crack closure. In: Fuentes, M., Martin-Meizoso, A., and Martinez-Esnaola, M. (eds.) *Frac. Mech.: Applications and Challenges*. Elsevier, Amsterdam (2000)
- [20] Gross, T.S., Mendelsohn, D.A.: Mode I Stress Intensity Factors Induced by Fracture Surface Roughness under Pure Mode III Loading : Application to the Effect of Loading Modes on Stress Corrosion Crack Growth. *Metall. Trans. A*. 20, (1989)
- [21] Vaziri, A., Nayeb-Hashemi, H.: The effect of crack surface interaction on the stress intensity factor in Mode III crack growth in round shafts. 72, 617-629 (2005). doi: 10.1016/j.engfracmech.2004.03.014
- [22] Gates, N., Fatemi, A.: Friction and roughness induced closure effects on shear-mode crack growth and branching mechanisms. *Int. J. Fatigue*. 92, 442-458 (2016). doi: 10.1016/j.ijfatigue.2016.01.023
- [23] Vojtek, T., Pokluda, J., Hohenwarter, A., Pippan, R.: Progress in understanding of intrinsic resistance to shear-mode fatigue crack growth in metallic materials. *Int. J. Fatigue*. (2016). doi: 10.1016/j.ijfatigue.2016.01.009
- [24] Pokluda, J., Trattnig, G., Martinschitz, C., Pippan, R.: Straightforward comparison of fatigue crack growth under modes II and III. *Int. J. Fatigue*. 30, 1498–1506 (2008). doi: 10.1016/J.IJFATIGUE.2007.09.009
- [25] Vojtek, T., Pippan, R., Hohenwarter, A., Holáň, L., Pokluda, J.: Near-threshold propagation of mode II and mode III fatigue cracks in ferrite and austenite. *Acta Mater.* 61, 4625–4635 (2013). doi: 10.1016/j.actamat.2013.04.033
- [26] Vojtek, T.: *Propagation of Fatigue Cracks under Shear Loading Modes II, III and II+III in the Near-threshold Region*. Brno: Vysoké učení technické v Brně, Fakulta strojního inženýrství, 2014. 72 p. Supervisor of the dissertation thesis prof. RNDr. Jaroslav Pokluda, CSc.
- [27] Richard, H.A.: A new compact shear specimen. *Int. J. Fract.* 17, R105–R107 (1981). doi: 10.1007/BF00033347
- [28] Plank, R., Kuhn, G.: Fatigue crack propagation under non-proportional mixed mode loading. *Eng. Fract. Mech.* 62, 203–229 (1999). doi: 10.1016/S0013-7944(98)00097-6
- [29] Horníková, J., Žák, S., Šandera, P.: K-calibration of special specimens for mode II, III and II+III crack growth. *Eng. Fract. Mech.* 110, 430–437 (2013). doi: 10.1016/j.engfracmech.2013.08.013

- [30] Richard, H.A., Benitz, K.: A loading device for the creation of mixed mode in fracture mechanics. *Int. J. Fract.* 22, R55–R58 (1983).
doi: 10.1007/BF00942726
- [31] Ansys Inc.: Ansys R17.2 help (user's manual), (2016)
- [32] Žák, S., Horníková, J., Šandera, P.: Shear mode stress intensity factors for serrated crack fronts. (2017). doi: 10.4028/www.scienti&c.net/KEM.754.214
- [33] Vojtek, T., Žák, S., Pokluda, J.: Quantitative analysis of intrinsic mode III fatigue thresholds in bcc metals. *Int. J. Fatigue.* (2018).
doi: 10.1016/j.ijfatigue.2018.04.022
- [34] Pokluda, J., Pippan, R., Vojtek, T., Hohenwarter, A.: Near-threshold behaviour of shear-mode fatigue cracks in metallic materials. *Fatigue Fract. Eng. Mater. Struct.* 37, 232–254 (2014). doi: 10.1111/ffe.12131
- [35] Vojtek, T., Pippan, R., Hohenwarter, A., Pokluda, J.: Prediction of effective mode II fatigue crack growth threshold for metallic materials. *Eng. Fract. Mech.* 174, 117–126 (2017). doi: 10.1016/j.engfracmech.2016.11.024
- [36] Vojtek, T., Žák, S., Pokluda, J.: Quantitative analysis of intrinsic mode III fatigue thresholds in bcc metals. *Int. J. Fatigue.* (2018).
doi: 10.1016/J.IJFATIGUE.2018.04.022
- [37] Milella, P.P.: *Fatigue and corrosion in metals.* (2013).
ISBN: 978-88-470-2336-9
- [38] Žák, S., Horníková, J., Šandera, P., Vojtek, T., Pokluda, J.: Stress Intensity Factors at In-plane and Out-of-plane Tortuous Crack Fronts under Remote Mode II Loading. *Frat. ed Integrità Strutt.* accepted (in print), (2018)
- [39] Žák, S., Horníková, J., Šandera, P., Vojtek, T., Pokluda, J.: Determination of Local Stress Intensity Factors at Microstructurally Tortuous Crack Fronts under Remote Mode II Loading. *Procedia Struct. Integr.* 5, (2017).
doi: 10.1016/j.prostr.2017.11.086
- [40] Vojtek, T., Pokluda, J., Šandera, P., Horníková, J., Hohenwarter, A., Pippan, R.: Analysis of fatigue crack propagation under mixed mode II+III in ARMCO iron. *Int. J. Fatigue.* 76, 47–52 (2015). doi: 10.1016/j.ijfatigue.2014.09.018
- [41] Vatne, I.R., Stukowski, A., Thaulow, C., Ostby, E., Marian, J.: Three-dimensional crack initiation mechanisms in bcc-Fe under loading modes I, II and III. *Mater. Sci. Eng. A.* 560, 306–314 (2013).
doi: 10.1016/j.msea.2012.09.071
- [42] Riemelmoser, F.O., Gumbsch, P., Pippan, R.: Dislocation Modelling of Fatigue Cracks: An Overview. *Mater. Trans.* 42, 2–13 (2001).
doi: 10.2320/matertrans.42.2
- [43] Žák, S., Horníková, J., Šandera, P.: Stress intensity factors for rough cracks loaded in mode II. *Solid State Phenomena* 258, (2017). doi: 10.4028/www.scienti&c.net/SSP.258.310

CURRICULUM VITAE

Personal details

Name Stanislav Žák
Date of birth 29. 1. 1990
Address Rouchovany 404, Rouchovany, 675 57, Czech Republic
E-mail stanislav.zak@ceitec.vutbr.cz

Education

2005 – 2009 Technical Lyceum, Secondary Technical School Třebíč (Manželu Curieových 734, Třebíč, 674 01, Czech Republic)
2009 – 2011 Engineering – Manufacturing Technology (bachelor's level), Brno University of Technology, Faculty of Mechanical Engineering (Technická 2896/2, Brno, 616 69, Czech Republic)
2011 – 2012 Engineering – Mechanical Engineering (bachelor's level), Brno University of Technology, Faculty of Mechanical Engineering (Technická 2896/2, Brno, 616 69, Czech Republic)
2012 – 2014 Applied Sciences in Engineering – Engineering Mechanics and Biomechanics (master's level), Brno University of Technology, Faculty of Mechanical Engineering (Technická 2896/2, Brno, 616 69, Czech Republic)
2014 – 2018 Advanced Materials and Nanosciences (Ph.D. study), Brno University of technology, Central European Institute of Technology (Purkyňova 123, Brno, 612 00, Czech Republic)

Career overview

4th October 2015 – 12th December 2015 Study/work internship at Fraunhofer IKTS, Dresden, Germany
1st January 2016 – 31st December 2018 Technical laborer (FE calculations) at CEITEC, BUT, Brno, Czech Republic
1st October 2016 – 30th June 2018 Calculation support at Fraunhofer IKTS, Dresden, Germany

Language skills

Czech (excellent/native speaker), English (intermediate), German (basic/passive), Russian (basic/passive)

Computer skills

Ansys, Matlab, Autodesk Inventor, Microsoft office (MS Word, Powerpoint, Excel)

Driving license

Category B – passenger car

ABSTRACT

The first part of the thesis topics contains a brief summary of the theoretical background of the fracture mechanics, whereas its methods enable complex evaluation of crack parameters and the influence of the crack. It is followed by the specification of aims of dissertation.

Subsequently the originally used methods and obtained results are concisely discussed. Models for two types of real specimens are shown (cylindrical specimen with the circumferential notch and crack and CTS specimen) implementing newly used crack front and flanks tortuosity. Moreover, the results complementing the knowledge of the fracture mechanics in the field of micro-structurally complicated cracks under the shear modes loading are described.

In the end, a full conclusion is given, relating to the results of the whole research (complementing present knowledge on the geometrical shielding effects), summarizing the whole extend of the dissertation thesis.

Reader should keep in mind, that only the main and the most important sections of full dissertation thesis are shown in these topics. Therefore, this publication presents the core of results and methods obtained during whole doctoral studies.

ABSTRAKT

První část práce je tvořena stručným shrnutím teoretického základu lomové mechaniky, jejíž metody umožňující komplexní určení hodnot součinitelů intenzity napětí a J -integrálu jsou použity na stanovení vlivu mikrostruktury trhliny. Následují hlavní cíle disertační práce.

Dále jsou popsány metody zvolené (a vytvořené) k získání hodnot součinitelů intenzity napětí, včetně diskuze výsledků. Prezentovány jsou dva konečno-prvkové modely reálných experimentálních těles (válcový vzorek s obvodovým vrubem a trhlinou a CTS těleso), u kterých je nově implementována drsnost lomových ploch a zubatost čela trhliny. Dále jsou zde popsány výsledky doplňující současné chápání vlivu geometrické mikrostruktury čela trhliny při zatěžování ve smyku.

Na závěr jsou všechny výsledky vyhodnoceny a shrnuty a ze získaných poznatků jsou vyvozeny závěry doplňující současné poznání geometrického stínění čela trhliny.

Tato zkrácená verze disertační práce obsahuje pouze nejdůležitější části plné disertační práce a představuje jádro výzkumu, provedeného v průběhu celého doktorského studia.